J Mater Sci: Mater Electron (2016) 27:8279–8287
DOI 10.1007/s10854-016-4834-5

Mechanical, thermal conductive and dielectrical properties of organic montmorillonite reinforced benzoxazine/cyanate ester copolymer for electronic packaging

Yiqun Wang[1] · Guanglei Wu[1,2] · Kaichang Kou[1] · Chen Pan[1] · Ailing Feng[3]

Received: 1 March 2016 / Accepted: 13 April 2016 / Published online: 18 April 2016

Abstract In this work, benzoxazine/bismaleimide/cyanate ester (BOZ/BMI/BADCy) was prepared by bisphenol A benzoxazine, bisphenol A dicyanate, 4, 4′-bismaleimidodiphenyl methane, and organo-modified 2D montmorillonite (OMMt) nanoparticles. OMMt was synthesized and characterized using FTIR. The effect of different weight fraction of OMMt (0–5 wt%) on the dielectric, thermal, mechanical properties of the composites was investigated. All composites exhibited excellent dielectric properties and thermal stability endowed by BOZ/BMI/BADCy matrix. OMMt improves their dispersibility, alignment and interfacial strength and hence electrical conductivity and real permittivity increase with increasing OMMt loading, and a suitable addition of OMMt can enhance the mechanical properties, dielectric strength as well as reduce the dielectric loss of BOZ/BMI/BADCy terpolymer. The dielectric constant and dielectric loss of the sample with 4 wt% of OMMt filler was 3.56 and 0.004, at 1 kHz. The dielectric constant of the composites showed only a very small variation with frequency in the range 100–1 MHz. All these changes in properties are closely correlated to the OMMt/BOZ/BMI/BADCy nanocomposites, which could form an interaction interface structure in the system.

✉ Guanglei Wu
wuguanglei@mail.xjtu.edu.cn

✉ Ailing Feng
ailing@mail.xjtu.edu.cn

[1] The Key Laboratory of Space Applied Physics and Chemistry, Ministry of Education and Shaanxi Key Laboratory of Macromolecular Science and Technology, School of Science, Northwestern Polytechnical University, Xi'an 710129, People's Republic of China

[2] Institute of Energy and Environmental Materials, Growing Base for State Key Laboratory, College of Materials Science and Engineering, Qingdao University, No. 308 Ningxia Road, Qingdao 266071, People's Republic of China

[3] Institute of Physics and Optoelectronics Technology, Baoji University of Arts and Sciences, Baoji 721016, People's Republic of China

1 Introduction

With the rapid development of the electronics industry, there has been an ever increasing demand for high-performance dielectric materials. For microelectronic packaging application, dielectric materials, and microwave absorbing materials with a suitable dielectric constant, low dielectric loss, high thermal conductivity and good thermal stability are required [1–5]. At present, such materials are mainly ceramics, which have drawbacks, such as high brittleness, low dielectric strength, high processing temperature and high density [6–12]. Thermosetting cyanate polymers have been widely used as matrices in fibre-reinforced polymer composites and in adhesive applications because of their high rigidity, strength, and chemical and thermal resistance [13, 14]. However, certain polymer-related applications require higher material performance. Cyanate ester resin is a well-known thermosetting resin with high thermal properties, low dielectric constant and high glass transition temperature after being fully cured to form a triazine network [15–18]. Polybenzoxazines have evinced significant interest as a class of high performance phenolic resin which combines the thermal properties and ame retardance of phenolics, with the mechanical performance and design exibility of epoxies [19–22]. The curing procedure of the benzoxazine-cyanate-epoxy system and the properties of the terpolymer were studied by Li et al. [23]. In our previous works [24–27], we reported that a

terpolymerzation between the cyanate ester, bismaleimide and benzoxazine resin and postulated a triazine-ether-benzoxazine network. Moreover, improving the dielectric properties of such polymers is necessary as insulating material [28, 29]. Compared with the matrix composite materials, the nanocomposites display much superior properties due to its low filling density, nano-scale grain and large specific surface area [30, 31]. The advent of nanotechnology and the promise of high interfacial area in nanocomposites energized research in socalled nanodielectrics; researchers saw the opportunity to surpass dielectric behavior predicted by effective media approaches and potentially achieve significant improvement in not only dielectric permittivity and breakdown strength but also in mechanical properties [32–34]. It has been reported recently in many papers that nanofillers such as zinc oxide [35, 36], titanium [37], silicon oxide [38, 39], have abviously improved electric properties of polymer, including conductivity, space charge behavior, breakdown strength, dielectric constant and electric tree [40–42]. However, dielectric constant was improved and,at the same time,dielectric loss also often was increased because of more interface polarization between nanofillers and polymer. Therefore, a type of nanofillers that need to be fabricated can improve dielectric constant and keep dielectric loss as low as possible.

Montmorillonite (MMT) is a type of clay with a laminated structure, in which the layers have the thickness of 1 nm. For the synthesis of a potent polymer/MMT nanocomposite, clay particles are usually modified via growth of the basal (interlayer) spacing by exchanging the metal cations with an intercalating reagent such as alkyl ammonium ions. This will facilitate intercalation of polymer chains into the galleries between the clay layers, decrease interactions between the MMT platelets, and improve the interaction between the polymer and the clay. Yang et al. [43] reported that the low density polyethylene/MMT composite after the electrically induced treatment showed higher capability for suppressing electrical trees under the power frequency field. Li et al. investigated XLPE/OMMT nanocomposites and the properties of the nanocomposites. The results showed that the addition of OMMT increases the storage modulus of all nanocomposites in the high temperature range and increases the relative dielectric constant of XLPE/OMMT composite, and also the tanδ [44]. It was found that introduction of organically treated clay improved the compatibility of the nanofiller with BADCy altering the nanodispersion dramatically from intercalation to exfoliation and affecting the final flammability properties. Moreover, it was established that dispersion degree of organoclay strongly depended on affinity between the chemical structures of clay modifier and BADCy monomer used.

In this study, nanocomposites were prepared and studied by incorporating organo-modified montmorillonite (OMMt) in BOZ/BMI/BADCy resins. The basic mechanical, thermal, dielectric, and fracture properties of the OMMt toughened polymers were investigated, and the degree of dispersion of the OMMt was examined by observing the morphology of nanocomposite bulk samples.

2 Experimental details

2.1 Materials

The montmorillonite(MMt) used was obtained from the Zhejiang Fenghong New Material Co. Ltd. without further purification. Octadearyl dimethyl ammonium chloride (OTAC) (purity > 99.5 %) was purchased from Xiamen Pioneer Technology Co., Ltd. (Xiamen, China). Bisphenol A dicyanate (BADCy) ester (purity > 99.5 %) white granular crystal was purchased from Shangyu Shengda Biochemical Co. Ltd. (Shangyu, China). 4, 4′-Bismaleimid odiphenyl methane (BMI) was purchased from Hubei Fengguang Chemicals, China. Bisphenol A benzoxazine (BOZ) was synthesized from bisphenol A, aniline and paraformaldehyde according to procedures previously described [45]. Paraformaldehyde, aniline, Bisphenol-A, acetone, and chloroform were purchased from Shanghai First Reagent Company (China). All chemicals were AR grade and used as-received. The chemical structures of BADCy, BMI and BOZ are shown in Fig. 1.

2.2 Preparation of OMMt/BOZ/BMI/BADCy nanocomposites

The montmorillonite (7.5 g) and H_2O (100 ml) were added into a 250 mL three-necked round bottomed flask, and then the mixture was maintained with stirring for 0.5 h at 60 °C and a homogeneous liquid was obtained. Then OTAC (2.4 g) was added into the flask at 60 °C for 2 h with vigorous stirring. After that, cooling the mixture to room temperature, obtained precipitate was centrifuged and washed several times with anhydrous ethanol and distilled water and dried in a vacuum oven at 70 °C for 15 h to obtain organo-modified montmorillonite (OMMt).

First, weight a certain amount of OMMt particle and pour it into beaker, and add acetone (20 mL) to the beaker of OMMt and then dispersed through ultrasonication for 0.5 h. Then, appropriate quantities of BADCy and BMI were placed in a three-necked flask with a mechanical stirrer and a thermometer. The mass ratios of BADCy and BMI were 4:3. The mixture was heated to 160 °C and maintained at that temperature with stirring until the homogeneous liquid was obtained. The liquid was

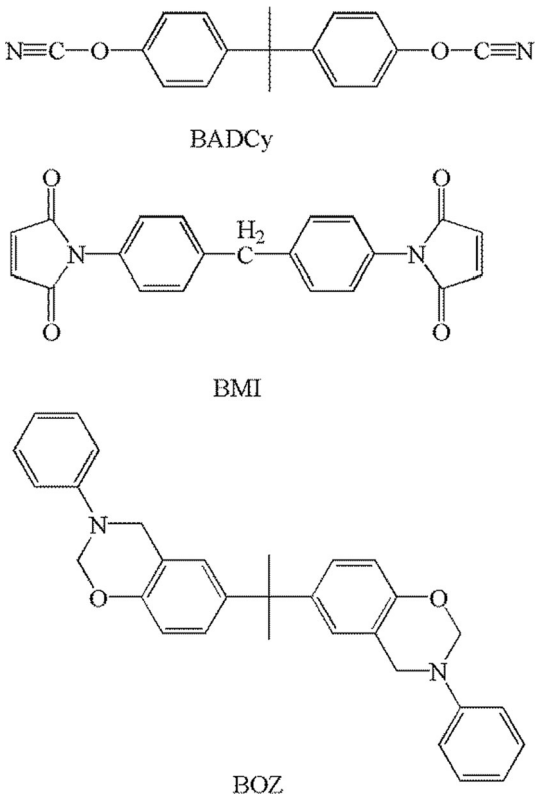

Fig. 1 Structures of BADCy, BMI and BOZ

maintained at that temperature for additional 0.5 h, which is BMI/BADCy prepolymer. After that, cooling the mixture to 140 °C the BOZ and OMMt solution was added, and then the ternary mixture was maintained with stirring for 20 min and a brown–red transparent liquid was obtained. Then the mixture was put into a preheated mold with release agent followed by degassing at 140 °C for 2 h in a vacuum oven. After that the mixture was cured and post-cured via the procedures of 150 °C/2 h + 180 °C/3 h + 200 °C/2 h, and post-cured at 240 °C/2 h. Finally, the mold was cooled to room temperature and demolded to get the samples of OMMt/BOZ/BMI/BADCy system. OMMt was blended with BOZ/BMI/BADCy in different mass ratios of 0, 1, 2, 3, 4 and 5 %. The nanocomposites were noted as u-OMMt, OMMt1, OMMt2, OMMt3, OMMt4 and OMMt5, respectively.

2.3 Characterization

FT-IR spectra were recorded on KBr pellets from 400 to 4000 cm^{-1} with a resolution of 4 cm^{-1} on a Nicolet IS10 IR spectrometer (USA). Thermogravimetric analysis (TGA) was performed on a NETZSCH TG209 F3 instrument (heating the composites from 50 to 800 °C with a rate of 10 °C/min in N_2 atmosphere). Scanning electron microscopy (SEM) images were recorded using a JEOL JEM 7401F field-emission scanning electron microscope. All samples were prepared by fracturing the composites at liquid nitrogen temperature and then sputter-coated with a homogeneous gold layer to avoid accumulation of charges. The dielectric properties of composites were tested by using a broadband dielectric spectrometer (CONCEPE 80, Novocontrol Technology Company, Germany) with an Alpha-A high-performance frequency analyzer over the frequency range of 10^{-1}–10^{6} Hz. The thermal diffusivity (δ) and specific heat (C) were measured on disk samples by using a LFA447 light flash system (NETZSCH, Selb, Germany) at 25 °C. The volume resistance (R_V) of the samples was measured by an Agilent 6517B high resistance meter after obtaining the thickness of these composites pellets. Mechanical properties were tested according to GB/T2567-2008.

3 Results and discussion

3.1 Structure and morphology analysis of the OMMt

The FTIR spectra of MMT before and after modification are shown in Fig. 2. Before modification the band at 3610 cm^{-1} is assigned to the stretching vibrations of the -OH groups bonded to the aluminum and/or silicon in the MMT interlayer. The broad band at 3460 cm^{-1} is assigned to the hydroxyl stretching vibrations, and the band at 1650 cm^{-1} corresponded to H–O–H bending vibrations shows the presence of some moisture in the samples. While for the samples after modification the new appearing bands at 2916 and 2853 cm^{-1} are attributed to asymmetric and symmetric C–H stretching vibrations of OTAC. The peak

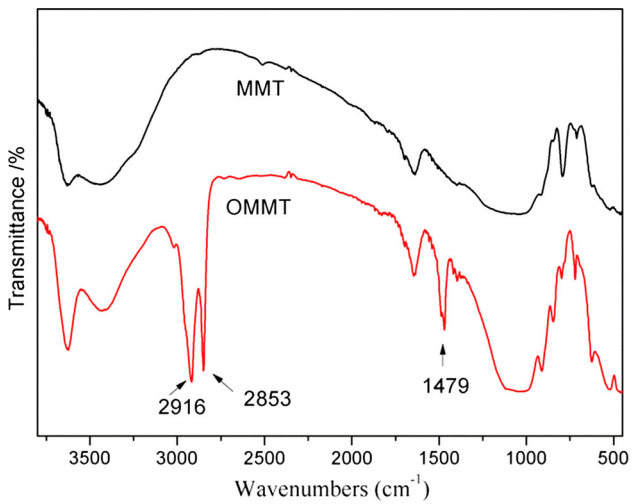

Fig. 2 FTIR spectra of MMT before and after modification

at 1479 cm^{-1} is attributed to the CH_3–N^+ moiety. Besides, the peaks at 1050 and 610 cm^{-1} result from the stretching vibration of Si–O and Al–O bonds in the MMT structure have no obvious change, which suggests that the main bones of MMT clay before and after modification are similar.

3.2 Mechanical properties of OMMt/BOZ/BMI/BADCy nanocomposites

The tensile strength, impact and flexural strengths of the OMMt/BOZ/BMI/BADCy nanocomposites are listed in Fig. 3 and Table 1. The addition of OMMt to the BOZ/BMI/BADCy increases the tensile strength, impact and flexural strengths at room temperature. It is observed from Fig. 3 that the MMt4 has the maximum impact strength (20.2 kJ/m^2), which is increased by 53 % compared with that of BOZ/BMI/BADCy. And tensile and flexural strengths of OMMt4 are 75.4 and 119 MPa, respectively, which is increased by 39 and 21 % compared with that of BOZ/BMI/BADCy resin, respectively. It is well known that the size, content, and interface interaction of rigid particles will have complex effects on the mechanical properties of resins. Interface interaction is particularly important when the size and content of nanoparticles are certain [46]. The organo-modified montmorillonite can improve interface interaction, which results in the efficient load transfer from the BOZ/BMI/BADCy matrix to the OMMt. The increased dispersibility of OMMt in BOZ/BMI/BADCy matrix is the most important factor for determining the mechanical properties of the composites. In our experiment, we prepared OMMt/BOZ/BMI/BADCy nanocomposites employing the method of melt casting and then curing. This process has the extent of reactions between OMMt and BOZ/BMI/BADCy, thus leading to improved interfacial bonding strength between OMMt and matrix. For the OMMt/BOZ/BMI/BADCy system, the probability of forming a strong organic–inorganic and organic–organic combination will be enhanced. Therefore, the mechanical properties of OMMt/BOZ/BMI/BADCy system are increased as the contents of OMMt from 0 to 4 wt%. However, when the fillers content is high enough (>4 wt%), the mechanical properties of the nanocomposites decrease with the increasing concentration of fillers. This occurs because further loading causes the OMMt to stack together, reducing the improvement return in mechanical properties [47].

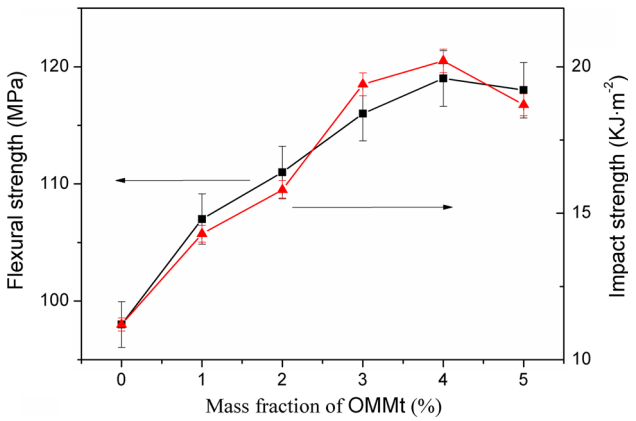

Fig. 3 The mechanical properties of OMMt/BOZ/BMI/BADCy nanocomposites with different content of OMMt

In order to further confirm the effect of OMMt on the toughness of BOZ/BMI/BADCy resin, SEM images of the fracture surfaces of samples after impact tests are taken and shown in Fig. 4, it can be observed that u-OMMt resin has a river-like fracture surface (Fig. 4a), exhibiting a typical brittle feature. While with the addition of OMMt into BOZ/BMI/BADCy resin, the fracture surfaces are accompanied with more ductile sunken areas, which is consistent with the improved impact strength of the nanocomposites. It is noted that the fracture surfaces of 1 and 4 wt% OMMt/BOZ/BMI/BADCy systems showed uniform dispersion and distribution of nanoparticles throughout BOZ/BMI/BADCy matrix, which suggests that the appropriate amount of OMMt has well compatibility with BOZ/BMI/BADCy matrix. Figure 4e indicates that OMMt was homogenously dispersed in BOZ/BMI/BADCy matrix. It is believed that organo groups present on the surfaces of MMt and OMMt might act as effective surfactants, leading to sufficient degree of distribution via secondary chemical attraction of these groups to BOZ/BMI/BADCy matrix. However, when the concentration of OMMt is 5 wt%, as shown in Fig. 4f, large clusters in the matrix appear due to the aggregation of OMMt at high concentration, which will lead to more rapid crack initiation and impact failure. Therefore, the impact strength of the nanocomposite with high OMMt content is decreased. The features of the fracture surfaces of OMMt/BOZ/BMI/BADCy systems accord well with the mechanical properties.

3.3 Dynamic mechanical analysis of OMMt/BOZ/BMI/BADCy nanocomposites

DMTA can characterize the viscoelastic properties of materials and determine the storage modulus and tan delta of the BOZ/BMI/BADCy and its nanocomposites; the results are shown in Figs. 5, 6 and Table 1. Clearly, the incorporation of the OMMt into BOZ/BMI/BADCy resin produces increased storage modulus in the glassy state. For the OMMt/BOZ/BMI/BADCy nanocomposites, this result may be ascribed to the fact that, below T_g, the rigid polymer matrix can exert large forces on the agglomerates, causing some particle motion and slippage, and a decrease

Table 1 The mechanical properties of OMMt/BOZ/BMI/BADCy nanocomposites with different content of OMMt

OMMt content	Sample ID	Flexural strength (MPa)	Flexural modulus (GPa)	Impact strength (kJ m^{-2})	Tensile strength (MPa)
0	u-OMMt	98	3.89	13.2	54.1
1 wt%	OMMt1	107	3.97	15.1	60.9
2 wt%	OMMt2	111	4.06	16.8	66.2
3 wt%	OMMt3	116	4.11	19.4	70.8
4 wt%	OMMt4	119	4.21	20.2	75.4
5 wt%	OMMt5	118	3.86	18.7	64.5

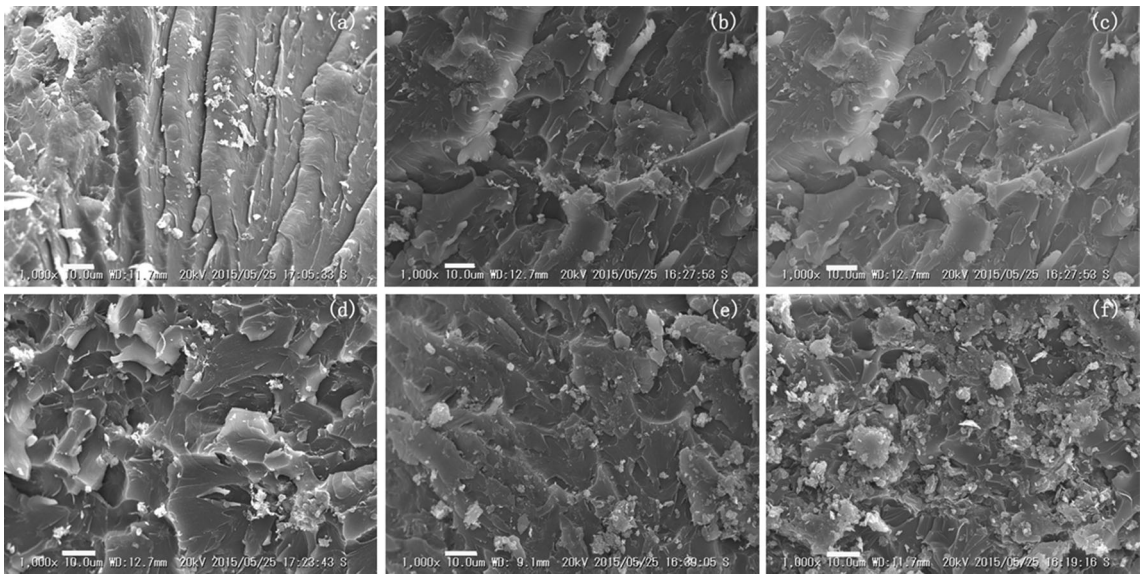

Fig. 4 SEM of fracture surfaces of OMMt/BOZ/BMI/BADCy nanocomposites with different content of OMMt (**a** 0 wt%, **b** 1 wt%, **c** 2 wt%, **d** 3 wt%, **e** 4 wt%, **f** 5 wt%)

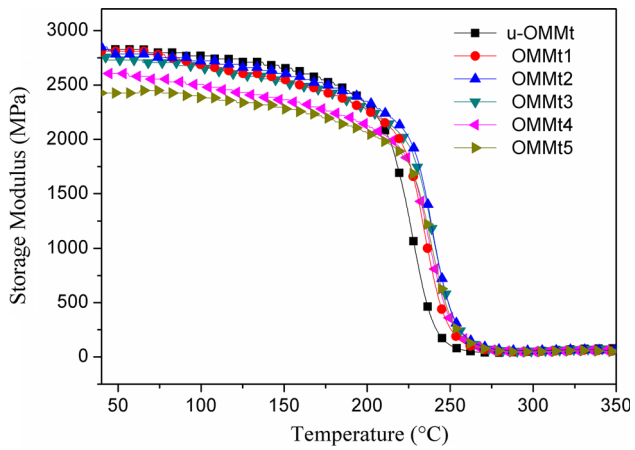

Fig. 5 The storage modulus of OMMt/BOZ/BMI/BADCy nanocomposites with different content of OMMt

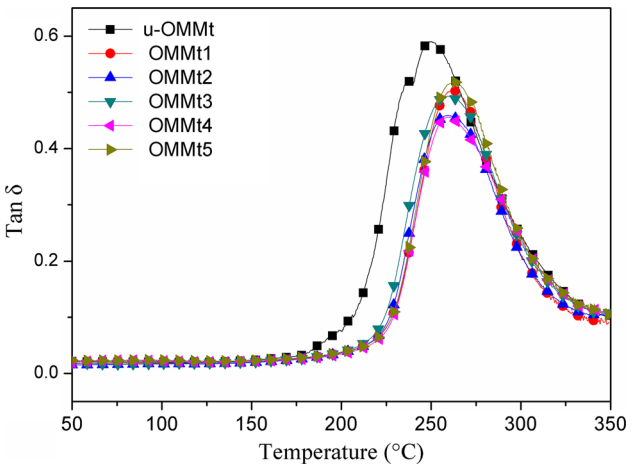

Fig. 6 The tanδ of OMMt/BOZ/BMI/BADCy nanocomposites with different content of OMMt

in storage modulus [48]. However, it is interesting to find that the OMMt/BOZ/BMI/BADCy nanocomposites at higher temperature tend to have higher storage moduli than unfilled OMMt. This phenomenon can be mainly interpreted by the different morphologies of the composites under different temperatures. In the rubbery state, BOZ/

BMI/BADCy become elastomers so that the chain segments can move freely. Consequently, the storage moduli of the composites are determined by those of fillers and the interface forces between the matrix and fillers. Interfacial adhesion between BOZ/BMI/BADCy and OMMt particles is expected to be very strong. Therefore, the motions of chain segments may intensively interact with the OMMt particles, leading to increased storage moduli at higher temperature.

Since the tan δ peak occurs in a temperature range over which the polymer changes from a glassy state to an elastic state, hence the peak temperature of which is often taken as the glass transition temperature (T_g) of a polymer. In this paper, the temperature corresponding to tan δ peak is considered as the T_g of the materials. T_gs of unfilled OMMt, OMMt1, OMMt2, OMMt3, OMMt4, and OMMt5 are 249.8, 259.2, 261.3, 262.5, 263.6, and 264.7 °C, respectively, as shown in Table 2. It indicates that the addition of OMMt into BOZ/BMI/BADCy resin can increase the T_g of BOZ/BMI/BADCy resin, and in the case of filling the same content of OMMt, T_g of the composite will be increased with the better dispersion of OMMt in matrix, in other words, the thermal property of the composite will be improved with the increasing homogeneity of the nanocomposites.

3.4 Thermal conductivity of OMMt/BOZ/BMI/BADCy nanocomposites

Figure 7 shows the variation of thermal conductivity of OMMt/BOZ/BMI/BADCy system as a function of temperature. The effective thermal conductivity for the terpolymer of BOZ/BMI/BADCy was found to be 0.195 Wm^{-1} K^{-1} at 25 °C and increases with temperature over the temperature range investigated. The thermal conductivity of OMMt/BOZ/BMI/BADCy nanocomposites exhibits temperature dependences similar to the terpolymer of BOZ/BMI/BADCy. Meanwhile, the thermal conductivity of OMMt/BOZ/BMI/BADCy nanocomposites increases with increasing OMMt content for all samples. The OMMt5 has the maximum thermal conductivity (0.248 Wm^{-1} K^{-1} at 25 °C), which is increased by 27 % compared with that of u-OMMt. And the thermal conductivity of the OMMt5 tends to be more stable at the temperature

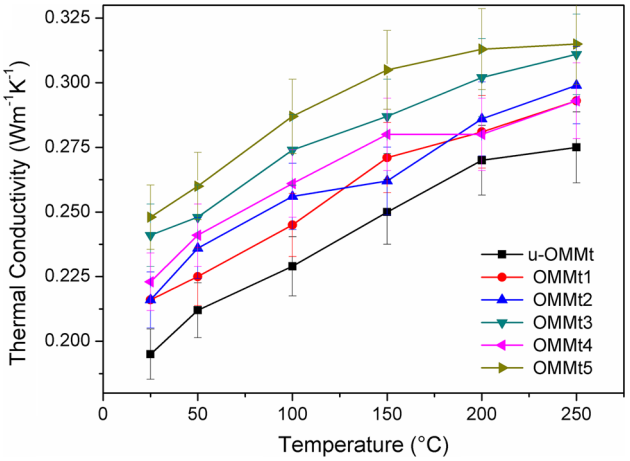

Fig. 7 The thermal conductivity of OMMt/BOZ/BMI/BADCy nanocomposites with different content of OMMt

increases. Various mechanisms have been presented to explain the increase of the effective thermal conductivity of composites containing different nanoparticles, such as interface interaction at the particle/resin interface [49], the nature of heat transport in the nanoparticles and the effects of nanoparticle clustering [50]. Based on our experimental results, it was concluded that the three dimensional network formed by OMMt/BOZ/BMI/BADCy nanocomposites dominates the thermal conduction mechanism, which leads to the composites with excellent thermal conductivity. Meanwhile, thermal conduction chains, the prevailing means to conduct thermal diffusion in the large-size filler/resin, are the secondary means to conduct thermal diffusion in the composites. The understanding of interface structure between OMMt and the matrix enables us to understand the thermal conduction mechanisms, therefore guides us to choose proper approaches to gain excellent thermal conductivity. Furthermore, it also leads us to design the novel nanocomposites with high thermal conductivity.

3.5 Thermal properties of the OMMt/BOZ/BMI/BADCy nanocomposites

In order to study the influence of the mass fraction of OMMt, samples have been analyzed by TGA. Figure 8 depicts TGA curves of polymer and nanocomposites. The content of OMMt in nanocomposites is 0, 1, 2, 3, 4 and

Table 2 Thermal properties of OMMt/BOZ/BMI/BADCy composites with different content of OMMt

Sample Content of OMMt	u-OMMt 0 wt%	OMMt1 1 wt%	OMMt2 2 wt%	OMMt3 3 wt%	OMMt4 4 wt%	OMMt5 5 wt%
T_{d5} (°C)	376	386	388	392	393	395
T_{d10} (°C)	387	394	395	400	402	403
Char yield (%)	45.21	45.94	45.99	46.03	46.95	48.03
T_g	249.8	259.2	261.3	262.5	263.6	264.7

5 wt%. As can be seen from Fig. 8, no obvious weight loss is detected before 350 °C, which was mainly due to the good thermal stability of BOZ/BMI/BADCy resin. The major weight loss was happened between 365 and 650 °C, which can be attributed to the degradation of macromolecular chain. The temperature with weight-loss of 5 wt% was defined as Initial degradation temperature (IDT), and IDT is increasing with increased OMMt in the nanocomposites as compared to the pure terpolymer. In Table 2, both the T_{d5} and T_{d10} of OMMt/BOZ/BMI/BADCy nanocomposites were higher, indicating that the nanocomposite has the best thermal stability. And the char yield at 800 °C is increasing with increased OMMt in the nanocomposites. One reason for this observation is that the thermal stability of OMMt is higher than the terpolymer, and higher OMMt content would increase the thermal stability of the composites.

3.6 Electric properties of OMMt/BOZ/BMI/BADCy nanocomposites

The volume resistivity of OMMt/BOZ/BMI/BADCy system was shown in Fig. 9. It can be seen from Fig. 9 that the volume resistivity of OMMt/BOZ/BMI/BADCy system is decreasing with increased OMMt at room temperature. As the content of OMMt increased, the level of conductivity of the composites tends to increase drastically due to the formation of the conducting bridges between the nanofiller and BOZ/BMI/BADCy. As the nanofiller loading further increase, the agglomeration of OMMt nanofillers in the composites becomes more apparent and it is more possible for the bridging between the electrodes to be formed, resulting in the increase of dc conductivity for OMMt/BOZ/BMI/BADCy nanocomposites. Furthermore, the cross-linked network structure between OMMt and the terpolymer has been formed, which is responsible for the high electrical conductivity of those samples.

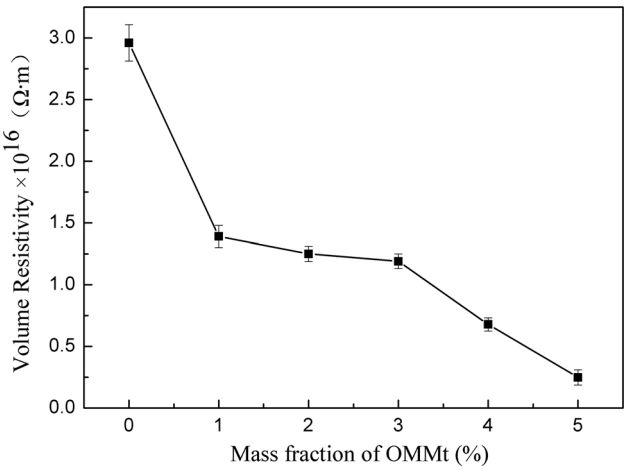

Fig. 9 The volume resistivity of OMMt/BOZ/BMI/BADCy nanocomposites with different content of OMMt

The frequency dependence of dielectric constant and dielectric loss for OMMt/BOZ/BMI/BADCy system was shown in Figs. 10 and 11. The dielectric constant at 1 MHz is 3.39 for OMMt5. It can be seen from Fig. 10 that the dielectric constant of OMMt/BOZ/BMI/BADCy system is decreasing with increased OMMt particles among the range of full frequency. There are two possible reasons. Firstly, the OMMt particles have lower dielectric constant than the terpolymer of BOZ/BMI/BADCy, which can cause dielectric constant of the composites to become small. Furthermore, the interfacial polarization can cause an decrease of dielectric constant in polymer composites when compared with the terpolymers. It is observed from Fig. 11 that the dielectric loss is increasing with increased OMMt particle among the range of low frequency, and

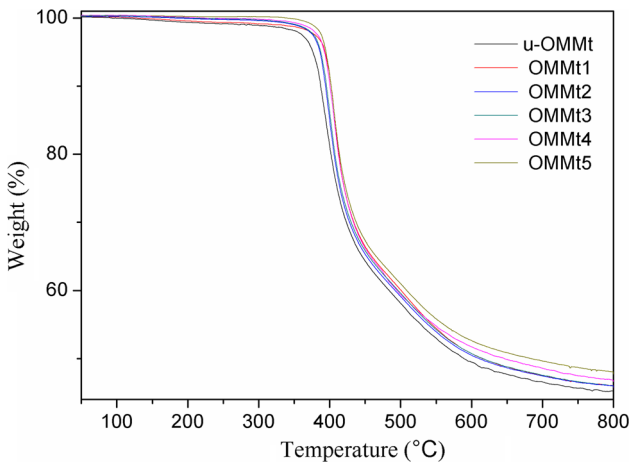

Fig. 8 TGA curves of the OMMt/BOZ/BMI/BADCy nanocomposites with different content of OMMt

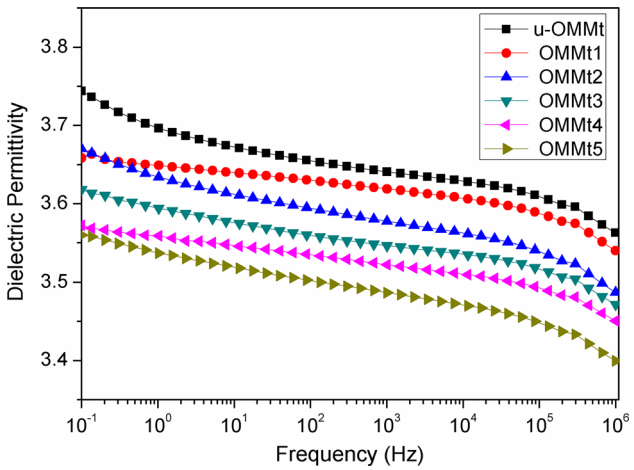

Fig. 10 The dielectric constant of OMMt/BOZ/BMI/BADCy nanocomposites with different content of OMMt

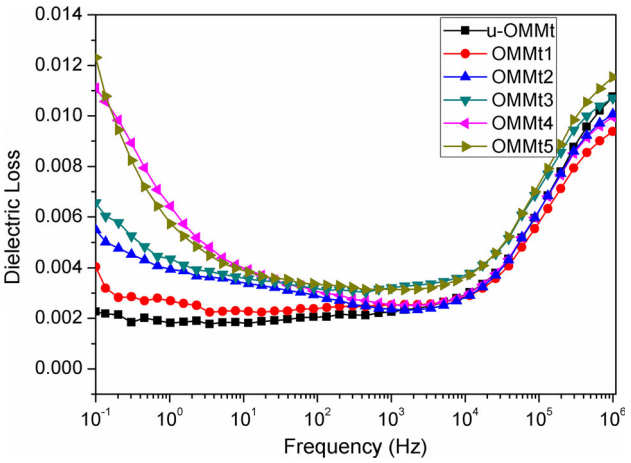

Fig. 11 The dielectric loss factor of OMMt/BOZ/BMI/BADCy nanocomposites with different content of OMMt

5 wt% loaded OMMt in copolymer show maximum value of 0.01154 at 1 MHz. However,the dielectric loss of composites with 4 wt% OMMt exhibit lower dielectric loss, and is close to the dielectric loss of composites with 2 wt% OMMt. The cause of this result is that high concent created the aggregation of the nanoparticles, which may cause interfacial polarization between OMMt and matrix to reduce.

4 Conclusions

In this paper, the OMMt particle is utilized to achieve a uniform dispersion of nano-sized OMMt particles in the BOZ/BMI/BADCy matrix, which is significantly improved mechanical, thermal conductivity and electric properties of the BOZ/BMI/BADCy matrix. OMMt4 shows the maximum impact strength and flexural strength, which are 53 and 21 % higher than that of BOZ/BMI/BADCy resin, respectively. Compared with the terpolymer, the effective thermal conductivity of the composites was found to be 0.248 Wm^{-1} K^{-1} at 25 °C, which is increased by 27 %,and the T_g value of MMt5 is 264.7 °C. The OMMt/BOZ/BMI/BADCy nanocomposites still shows higher value of IDT. The BOZ/BMI/BADCy resin with OMMt still shows good thermal resistance. Meanwhile, a suitable addition of OMMt can improve the dielectric properties of BOZ/BMI/BADCy resin. The dielectric constant and loss of the composites with 5 wt% OMMt are from 3.38 to 3.56 and 0.0033 to 0.0123 over a relatively wide frequency band from 10^{-1} to 10^{6} Hz, respectively. In addition, the volume resistivity of BOZ/BMI/BADCy resin and OMMt/BOZ/BMI/BADCy is decreasing with increased OMMt at room temperature. The SEM analysis shows that the nanocomposites have a distinct characteristic of ductile fracture.

Acknowledgments This work was financially supported by National Natural Science Foundation of China (No. 51407134), China Postdoctoral Science Special Foundation (No. 2015T81028) and Natural Science Basic Research Plan in Shaanxi Province of China (Nos. 2014JQ6199, 2015JM5215).

References

1. C. Pan, K. Kou, G. Wu, Y. Zhang, J. Mater. Sci Mater. Electron. **27**, 286 (2016)
2. G. Wu, Y. Cheng, F. Xiang, Z. Jia, Mater. Sci. Semicond. Process. **41**, 6 (2016)
3. Y. Ren, H. Li, G. Wu, L. Yang, L. Wang, F. Ren, H. Wu, NANO **11**, 13 (2016)
4. H. Wu, G. Wu, Q. Wu, L. Wang, Mater. Charact. **97**, 18 (2014)
5. Z.M. Dang, J.K. Yuan, J.W. Zha, Prog. Mater Sci. **57**, 660 (2012)
6. H. Wu, G. Wu, L. Wang, Powder Technol. **269**, 443 (2015)
7. Q. Wu, G. Wu, L. Wang, W. Hu, H. Wu, Mater. Sci. Semicond. Process. **30**, 476 (2015)
8. G. Subodh, V. Deepu, P. Mohanan, Appl. Phys. Lett. **95**, 062903 (2009)
9. G. Wu, Y. Cheng, Y. Ren, Y. Wang, J. Alloy. Compd. **652**, 346 (2015)
10. F. Ren, G. Zhu, P. Ren, K. Wang, X. Cui, X. Yan, Appl. Surf. Sci. **351**, 40 (2015)
11. E.S. Kim, J.H. Shim, J.Y. Woo, J. Appl. Polym. Sci. **117**, 809 (2010)
12. H. Wu, G. Wu, Y. Ren, L. Yang, J. Mater. Chem. C. **3**, 7677 (2015)
13. A. Chaplin, I. Hamerton, B. Howlin, J. Barton, Macromolecules **27**, 4927 (1994)
14. C.P. Reghunadhan Nair, T. Francis, T. Vijayan, K. Krishnan, J. Appl. Polym. Sci. **74**, 2737 (1999)
15. M. SugunaLakshmi, B.S.R. Reddy, Eur. Polym. J. **38**, 795 (2002)
16. Y.Q. Wang, K.C. Kou, W. Zhao, G.L. Wu, F.L. Han, RSC Adv. **5**, 99313 (2015)
17. G. Wu, Y. Cheng, Q. Xie, C. Liu, J. Polym. Res. **21**, 615 (2014)
18. F. Ren, G.M. Zhu, Y.K. Wang, X.P. Cui, J. Polym. Res. **21**, 585 (2014)
19. B.S. Rao, A. Palanisamy, React. Funct. Polym. **71**, 148 (2011)
20. H. Ishida, D.J. Allen, J. Polym. Sci. Part B Polym. Phys. **34**, 1019 (1996)
21. G.L. Wu, K.C. Kou, M. Chao, L.H. Zhuo, Thermochim. Acta **537**, 44 (2012)
22. F. Ren, G. Zhu, P. Ren, Y. Wang, X. Cui, Appl. Surf. Sci. **316**, 549 (2014)
23. X. Li, Y. Xia, W. Xu, Q. Ran, Y. Gu, Polym. Chem. **3**, 1629 (2012)
24. G.L. Wu, Y.H. Cheng, K.K. Wang, J. Mater. Sci Mater. Electron. (2016). doi:10.1007/s10854-016-4464-y
25. Y. Wang, K. Kou, G. Wu, A. Feng, L. Zhuo, RSC Adv. **5**, 58821 (2015)
26. Y. Wang, K. Kou, G. Wu, L. Zhuo, J. Li, Y. Zhang, Polymer **77**, 354 (2015)
27. G. Wu, K. Kou, L. Zhuo, Y. Wang, J. Zhang, Thermochim. Acta **559**, 86 (2013)
28. R. Sarathi, R. Sahu, M.G. Danikas, J. Electr. Eng **60**, 358 (2009)
29. G. Wu, K. Kou, N. Li, H. Shi, M. Chao, J. Appl. Polym. Sci. **128**, 1164 (2013)
30. J. Zhang, E. Manias, C.A. Wilkie, J. Nanosci. Nanotechnol. **8**, 1597 (2008)
31. E. Manias, Nat. Mater. **6**, 9 (2007)
32. P. Kim, S.C. Jones, P.J. Hotchkiss, J.N. Haddock, B. Kippelen, S.R. Marder, J.W. Perry, Adv. Mater. **19**, 1001 (2007)

33. J.K. Nelson, J.C. Fothergill, Nanotechnology **15**, 586 (2004)
34. T. Tanaka, M. Kozako, N. Fuse, Y. Ohki, I.E.E.E. Trans, Dielectr. Electr. Insul. **12**, 669 (2005)
35. G. Wu, Y. Cheng, Q. Xie, Z. Jia, F. Xiang, H. Wu, Mater. Lett. **144**, 157 (2015)
36. E. Afsharmanesh, H. Karimi-Maleh, A. Pahlavan, J. Vahedi, J. Mol. Liq. **181**, 8 (2013)
37. R. Fleming, T. Pawlowski, A. Ammala, P. Casey, K. Lawrence, I.E.E.E. Trans, Dielectr. Electr. Insul. **12**, 745 (2005)
38. Y.Q. Li, Y. Yang, S.Y. Fu, X.Y. Yi, L.C. Wang, H.D. Chen, J. Phys. Chem. C **112**, 18616 (2008)
39. G.L. Wu, K.C. Kou, M. Chao, L.H. Zhuo, J. Wuhan, Univ. Technol. Mater. Sci. Ed. **28**, 261 (2013)
40. L. Fredin, Z. Li, M. Ratner, M. Lanagan, T. Marks, Adv. Mater. **24**, 5946 (2012)
41. F. Du, R. Scogna, W. Zhou, S. Brand, J. Fischer, K. Winey, Macromolecules **37**, 9048 (2004)
42. S. Rimdusit, H. Ishida, Polymer **41**, 7941 (2000)
43. L. Yang, G. Bai, Y. Liu, J. Gu, J. Li, H. Zhang, I.E.E.E. Trans, Dielectr. Electr. Insul. **22**, 1684 (2015)
44. X. Li, M. Xu, K. Zhang, D. Xie, X. Cao, X. Liu, I.E.E.E. Trans, Dielectr. Electr. Insul. **21**, 1705 (2014)
45. X. Ning, H. Ishida, J. Polym. Sci. Part A Polym. Chem. **32**, 1121 (1994)
46. Q. Jia, M. Zheng, C. Xu, H. Chen, Polym. Adv. Technol. **17**, 168 (2006)
47. Q. Wang, L. Zhu, J. Polym. Sci. Part B Polym. Phys. **49**, 1421 (2011)
48. W.K. Goertzen, M. Kessler, Compos. Part A. Appl. Sci. **39**, 761 (2008)
49. H. Okubo, I.E.E.E. Trans, Dielectr. Electr. Insul. **19**, 733 (2012)
50. J. Shang, Y. Zhang, L. Yu, B. Shen, F. Lv, P.K. Chu, Mater. Chem. Phys. **134**, 867 (2012)